



Pergamon

Acta mater. 49 (2001) 1879–1890



www.elsevier.com/locate/actamat

## A PHASE-FIELD MODEL FOR EVOLVING MICROSTRUCTURES WITH STRONG ELASTIC INHOMOGENEITY

S. Y. HU and L. Q. CHEN<sup>†</sup>

Department of Materials Science and Engineering, The Pennsylvania State University, University Park, PA 16802, USA

( Received 17 July 2000; received in revised form 15 March 2001; accepted 15 March 2001 )

**Abstract**—An efficient phase-field model is proposed to study the coherent microstructure evolution in elastically anisotropic systems with significant elastic modulus inhomogeneity. It combines an iterative approach for obtaining the elastic displacement fields and a semi-implicit Fourier–spectral method for solving the time-dependent Cahn–Hilliard equation. Each iteration in our iterative numerical simulation has a one-to-one correspondence to a given order of approximation in Khachatryan’s perturbation method. A unique feature of this approach is its ability to control the accuracy by choosing the appropriate order of approximation. We examine shape dependence of isolated particles as well as the morphological dependence of a phase-separated multi-particle system on the degree of elastic inhomogeneity in elastically anisotropic systems. It is shown that although prior calculations using first-order approximations correctly predicted the qualitative dependence of a two-phase morphology on elastic inhomogeneity, the local stress distributions and thus the driving force for microstructure evolution such as coarsening were in serious error quantitatively for systems with strong elastic inhomogeneity. © 2001 Acta Materialia Inc. Published by Elsevier Science Ltd. All rights reserved.

**Keywords:** Diffusion, interface; Microstructure; Phase field; Elastic

### 1. INTRODUCTION

Essentially all solid–solid phase transformations produce coherent microstructures at their early stages. In a coherent microstructure, the lattice directions and planes are continuous across the interfaces separating the parent and product phases or separating different orientation domains of the product phase. In order to maintain this lattice continuity, the lattice mismatch between the product and the parent phases and among the orientation domains of the product phase is accommodated by elastic displacements of atoms from their equilibrium lattice positions. Therefore, formation of coherent microstructures generates elastic strain energy whose magnitude depends on the degree of lattice mismatch, the elastic properties of each phase, and the shape and spatial distributions of coherent domains [1, 2].

The effect of elastic strain energy on coherent precipitate morphology and its temporal evolution has been a subject of extensive experimental and theoretical studies, for reviews see [3, 4]. Most of the existing theoretical analysis and numerical modeling of elastic

effect assumed that the elastic modulus is homogeneous [5–22], or that the modulus inhomogeneity is small so that first-order approximations may be employed [23–30].

There have been a number of approaches proposed for modeling the elastic effect on precipitate morphology in coherent systems with a significant elastic inhomogeneity. For example, Lee proposed a discrete atom method (DAM) which allows rather arbitrary elastic inhomogeneity and precipitate morphology [31, 32]. Due to the discrete nature of the method, the spatial scale of the precipitates described by this method is atomic. Schmidt and Gross [33, 34] studied the equilibrium shapes of a coherent precipitate using a boundary integral method and a sharp-interface description. In [33, 34], the temporal evolution of precipitate morphology through diffusion transport of atoms was not considered. Jou *et al.* examined the temporal evolution of precipitate shapes in elastically inhomogeneous systems by simultaneously solving a diffusion equation and the elasticity equation using the boundary integral method [35]. Since the interfaces are considered to be sharp, it is difficult to handle certain topological changes which take place, e.g., during initial stage of spinodal phase separation, and during precipitate coalescence and splitting. Leo *et al.* developed a diffuse-interface model for mode-

<sup>†</sup> To whom all correspondence should be addressed. Tel.: +1 814 863 8101; Fax: +1 814 863 0016.

E-mail address: chen@ems.psu.edu (L.Q. Chen)

ling elastically inhomogeneous systems by coupling the Cahn–Hilliard diffusion equation with an elasticity equation. In this method, the elasticity equation is numerically solved by a conjugate gradient method (CGM) at any given moment during microstructure evolution [36]. A similar diffuse-interface model using CGM is proposed by Zhu *et al.* [37].

Recently, Khachaturyan *et al.* developed an analytical solution for the elastic field in an elastically inhomogeneous system using a perturbation method (PM) and sharp-interface description [38]. The strain energy is expressed as a sum of multiparticle interactions between finite elements of the constituent phases, pairwise, triplet, quadriplet and so on, the  $n$ -particle interaction energy being related to the  $(n-2)$ th order term in the Taylor expansion of the Green function with respect to the elastic modulus misfit. The order of approximation required for a given system depends on the desired accuracy and the degree of elastic inhomogeneity. However, direct application of the analytical elastic energy expression to numerical simulation of coherent microstructure evolution in elastically inhomogeneous systems is difficult since the elastic strain energy involves multi-dimensional integrals in both real and Fourier spaces.

The main purpose of this paper is to present an efficient diffuse-interface phase-field model for elastically inhomogeneous systems. We used an iterative approach for numerically solving the elastic equilibrium equation and employed a diffuse-interface description. A unique feature of this method is the fact that each iteration in our numerical method corresponds to a given order of approximation in Khachaturyan’s perturbation method. To be consistent with [38], we will simply call our numerical method the “perturbation method” or PM. We will apply PM to elastically anisotropic coherent systems with strong elastic inhomogeneity and compare our results with those predicted previously by others using first-order approximations. Application of the proposed PM to calculating effective elastic modulus of a two-phase mixture and its temporal evolution will be discussed in a future publication.

## 2. ELASTIC ENERGY IN AN ELASTICALLY INHOMOGENEOUS SYSTEM IN DIFFUSE-INTERFACE DESCRIPTION

### 2.1. Mechanical equilibrium equation

We consider a simple binary solid solution with a compositional inhomogeneity described by  $X(\mathbf{r})$ , representing the mole or atom fraction  $X$  at position  $\mathbf{r}$ . We assume that the local elastic modulus tensor can be described in terms of the compositional inhomogeneity through

$$\lambda_{ijkl}(\mathbf{r}, t) = \lambda_{ijkl}^m \frac{(X_{\text{eq}}^p - X(\mathbf{r}))}{X_{\text{eq}}^p - X_{\text{eq}}^m} + \lambda_{ijkl}^p \frac{(X(\mathbf{r}) - X_{\text{eq}}^m)}{X_{\text{eq}}^p - X_{\text{eq}}^m} \quad (1)$$

where  $\lambda_{ijkl}^m$  and  $\lambda_{ijkl}^p$  are the elastic modulus tensors for the matrix with equilibrium composition  $X_{\text{eq}}^m$  and for the precipitate with equilibrium composition  $X_{\text{eq}}^p$ , respectively. It is easy to show that the local elastic modulus tensor (1) can be rewritten as

$$\lambda_{ijkl}(\mathbf{r}) = \lambda_{ijkl}^o + \lambda'_{ijkl} \delta X(\mathbf{r}) \quad (2)$$

where  $\delta X(\mathbf{r}, t) = X(\mathbf{r}, t) - X_o$ ,  $\lambda_{ijkl}^o$  is a constant representing the elastic modulus tensor for a homogeneous solid solution with composition  $X_o$ , and  $\lambda'_{ijkl}$  is given by

$$\frac{(\lambda_{ijkl}^p - \lambda_{ijkl}^m)}{(X_{\text{eq}}^p - X_{\text{eq}}^m)}$$

If we assume that the variation of stress-free lattice parameter,  $a$ , with composition obeys the Vegard’s law, the local stress-free strain caused by compositional inhomogeneity is given by,

$$\epsilon_{ij}^o(\mathbf{r}) = \epsilon_o \delta X(\mathbf{r}) \delta_{ij} \quad (3)$$

where  $\epsilon_o = (1/a)(da/dX)$  is the composition expansion coefficient of the lattice parameter and  $\delta_{ij}$  is the Kronecker–Delta function.

Let’s use  $\epsilon_{ij}(\mathbf{r})$  to denote the total strain measured with respect to a reference lattice and assume linear elasticity, the Hook’s law gives the local elastic stress,

$$\sigma_{ij}^{\text{el}}(\mathbf{r}) = [\lambda_{ijkl}^o + \lambda'_{ijkl} \delta X(\mathbf{r})][\epsilon_{kl}(\mathbf{r}) - \epsilon_{kl}^o(\mathbf{r})] \quad (4)$$

Since the mechanical equilibrium with respect to elastic displacements is established much faster than any diffusional processes, for any given distribution of composition, the system is always at mechanical equilibrium,

$$\frac{\partial \sigma_{ij}^{\text{el}}}{\partial r_j} = 0 \quad (5)$$

where  $r_j$  is the  $j$ th component of the position vector,  $\mathbf{r}$ . Following Khachaturyan [1], the total strain  $\epsilon_{ij}(\mathbf{r})$  may be represented as the sum of homogeneous and heterogeneous strains:

$$\epsilon_{ij}(\mathbf{r}) = \bar{\epsilon}_{ij} + \delta \epsilon_{ij}(\mathbf{r}) \quad (6)$$

where the homogeneous strain,  $\bar{\epsilon}_{ij}$ , is defined so that

$$\int_V \delta \epsilon_{ij}(\mathbf{r}) d^3 r = 0 \quad (7)$$

The homogeneous strain is the uniform macroscopic strain characterizing the macroscopic shape and volume change associated with the total strain,  $\epsilon_{ij}(\mathbf{r})$ . Let us use  $u_i(\mathbf{r})$  to denote the  $i$ th component of displacement. According to the relationship of strain and displacement, the heterogeneous strain can be expressed as,

$$\delta\epsilon_{kl}(\mathbf{r}) = \frac{1}{2} \left[ \frac{\partial u_k(\mathbf{r})}{\partial r_l} + \frac{\partial u_l(\mathbf{r})}{\partial r_k} \right] \quad (8)$$

Substituting equations (4), (8) and (6) to the mechanical equilibrium equation (5), one has

$$\begin{aligned} & \left[ \lambda_{ijkl}^{\circ} \frac{\partial^2}{\partial r_j \partial r_l} + \lambda'_{ijkl} \frac{\partial}{\partial r_j} \left( \delta X(\mathbf{r}) \frac{\partial}{\partial r_l} \right) \right] u_k(\mathbf{r}) \\ & = (\lambda_{ijkl}^{\circ} \epsilon_{kl}^{\circ} - \lambda'_{ijkl} \bar{\epsilon}_{kl}) \frac{\partial(\delta X(\mathbf{r}))}{\partial r_j} + \lambda'_{ijkl} \epsilon_{kl}^{\circ} \frac{\partial(\delta X(\mathbf{r}))^2}{\partial r_j} \end{aligned} \quad (9)$$

The determination of the equilibrium elastic field for an elastically inhomogeneous system is reduced to solving the mechanical equilibrium equation (9) subject to appropriate boundary conditions.

## 2.2. Solution to the mechanical equilibrium equation

**2.2.1. Zeroth-order approximation.** Because of the nonlinearity of the mechanical equilibrium equation (9), in general, it cannot be solved analytically. However, if one ignores the elastic modulus inhomogeneity,  $\lambda'_{ijkl} = 0$ , the mechanical equilibrium equation becomes linear and is given by

$$\lambda_{ijkl}^{\circ} \frac{\partial^2 u_k^{\circ}(\mathbf{r})}{\partial x_j \partial x_l} = \sigma_{ij}^{\circ} \frac{\partial \delta X(\mathbf{r})}{\partial x_j} \quad (10)$$

where  $u_k^{\circ}$  denotes the  $k$ th component of the displacement in the zeroth order approximation and  $\sigma_{ij}^{\circ} = \lambda_{ijkl}^{\circ} \epsilon_{kl}^{\circ}$ . Equation (10) can be readily solved in the Fourier space,

$$v_k^{\circ}(\mathbf{g}) = -i G_{ik}(\mathbf{g}) g_j \sigma_{ij}^{\circ} \delta X(\mathbf{g}) \quad (11)$$

where  $v_k^{\circ}(\mathbf{g})$  and  $\delta X(\mathbf{g})$  are Fourier transforms of  $u_k^{\circ}(\mathbf{r})$  and  $\delta X(\mathbf{r})$ , respectively,  $\mathbf{g}$  is a reciprocal lattice vector,  $g_j$  is the  $j$ th component of  $\mathbf{g}$ , and  $G_{ik}(\mathbf{g})$  is the inverse tensor to  $(G^{-1}(\mathbf{g}))_{ik} = g^2 \lambda_{ijkl}^{\circ} n_j n_l = g^2 \Omega_{ik}^{-1}(\mathbf{n})$  with  $\mathbf{n} = \mathbf{g}/|\mathbf{g}|$ . The back Fourier transform of  $v_k^{\circ}(\mathbf{g})$  gives the real-space solution for the displacement field in the zeroth order approximation,

$$u_k^{\circ}(\mathbf{r}) = \frac{1}{(2\pi)^3} \int v_k^{\circ}(\mathbf{g}) e^{i\mathbf{g}\cdot\mathbf{r}} d^3\mathbf{g} \quad (12)$$

**2.2.2. First-order approximation.** With the zeroth-order solution, one can analytically obtain the solution for the displacement field with a first-order approximation. To do this, we replace the displacement in the nonlinear term in equation (9) using the zeroth order solution and move it to the right-hand side,

$$\begin{aligned} & \lambda_{ijkl}^{\circ} \frac{\partial^2 u_k^{\circ}(\mathbf{r})}{\partial r_j \partial r_l} = (\sigma_{ij}^{\circ} \\ & - \lambda'_{ijkl} \bar{\epsilon}_{kl}) \frac{\partial(\delta X(\mathbf{r}))}{\partial r_j} + \lambda'_{ijkl} \epsilon_{kl}^{\circ} \frac{\partial(\delta X(\mathbf{r}))^2}{\partial r_j} \\ & - \lambda'_{ijkl} \frac{\partial}{\partial r_j} \left[ \delta X(\mathbf{r}) \frac{\partial u_k^{\circ}(\mathbf{r})}{\partial r_l} \right] \end{aligned} \quad (13)$$

where  $u_k^{\circ}(\mathbf{r})$  represents the  $k$ th component of displacement in the first-order approximation. Equation (13) has essentially the same structure as equation (10) except for a slightly more complicated right-hand side in equation (13). Therefore, the solution  $u_k^{\circ}(\mathbf{r})$  can also be analytically obtained using Fourier transforms, i.e.

$$\begin{aligned} v_k^1(\mathbf{g}) = & -i G_{ik}(\mathbf{g}) g_j \left[ (\sigma_{ij}^{\circ} \right. \\ & - \lambda'_{ijlm} \bar{\epsilon}_{lm}) \delta X(\mathbf{g}) + \lambda'_{ijlm} \epsilon_{lm}^{\circ} \{ (\delta X(\mathbf{r}))^2 \}_{\mathbf{g}} \\ & \left. - \lambda'_{ijlm} \left( \delta X(\mathbf{r}) \frac{\partial u_l^{\circ}(\mathbf{r})}{\partial r_m} \right)_{\mathbf{g}} \right] \end{aligned} \quad (14)$$

A significant difference between equation (10) and equation (13) is the fact that the homogeneous strain,  $\bar{\epsilon}_{ij}$  enters equation (13). As a result, with a first-order approximation, an applied strain or stress will affect the heterogeneous elastic displacements.

**2.2.3. High-order approximations.** Higher order solutions for  $u_k(\mathbf{r})$  can be derived using a similar approach as the first-order approximation. For example, the  $n$ th order solution for displacement,  $u_k^n(\mathbf{r})$ , can be obtained from the following equation,

$$\begin{aligned} & \lambda_{ijkl}^{\circ} \frac{\partial^2 u_k^n(\mathbf{r})}{\partial r_j \partial r_l} = (\lambda_{ijkl}^{\circ} \epsilon_{kl}^{\circ} \\ & - \lambda'_{ijkl} \bar{\epsilon}_{kl}) \frac{\partial(\delta X(\mathbf{r}))}{\partial r_j} + \lambda'_{ijkl} \epsilon_{kl}^{\circ} \frac{\partial(\delta X(\mathbf{r}))^2}{\partial r_j} \\ & - \lambda'_{ijkl} \frac{\partial}{\partial r_j} \left[ \delta X(\mathbf{r}) \frac{\partial u_k^{n-1}(\mathbf{r})}{\partial r_l} \right] \end{aligned} \quad (15)$$

where  $u_k^{n-1}(\mathbf{r})$  is the solution from a lower-order approximation. Again the elastic displacement in the  $n$ th order approximation can be obtained from equation (15) using Fourier transforms. Each of the successive orders of the approximation has a one-to-one correspondence to the order of approximation discussed by Khachaturyan *et al.* for elastically inhomogeneous systems with a sharp-interface description [38].

2.2.4. *Elastic energy in an elastically inhomogeneous system.* The coherency elastic strain energy density for a given compositional distribution in an elastically inhomogeneous and anisotropic system is given by

$$\begin{aligned}
e_{\text{el}} &= \frac{1}{2} \lambda_{ijkl} \epsilon_{ij}^{\text{el}} \epsilon_{kl}^{\text{el}} \\
&= \frac{1}{2} [\lambda_{ijkl}^{\circ} + \lambda'_{ijkl} \delta X(\mathbf{r})] \epsilon_{ij}^{\circ} \epsilon_{kl}^{\circ} (\delta X(\mathbf{r}))^2 \\
&\quad + \frac{1}{2} [\lambda_{ijkl}^{\circ} + \lambda'_{ijkl} \delta X(\mathbf{r})] \delta \epsilon_{ij} \delta \epsilon_{kl} \\
&\quad - [\lambda_{ijkl}^{\circ} + \lambda'_{ijkl} \delta X(\mathbf{r})] \epsilon_{ij}^{\circ} \delta \epsilon_{kl} \delta X(\mathbf{r}) \\
&\quad + \frac{1}{2} [\lambda_{ijkl}^{\circ} + \lambda'_{ijkl} \delta X(\mathbf{r})] \bar{\epsilon}_{ij} \bar{\epsilon}_{kl} \\
&\quad + [\lambda_{ijkl}^{\circ} + \lambda'_{ijkl} \delta X(\mathbf{r})] [\delta \epsilon_{ij} - \epsilon_{ij}^{\circ} \delta X(\mathbf{r})] \bar{\epsilon}_{kl}
\end{aligned} \tag{16}$$

The total coherency strain energy is given by

$$E_{\text{el}} = \int_V e_{\text{el}} d^3r \tag{17}$$

In equation (16),  $\delta \epsilon_{ij}(\mathbf{r})$  is given by

$$\delta \epsilon_{ij}(\mathbf{r}) = \frac{1}{(2\pi)^3} \int_2^i [v_i(\mathbf{g}) g_j + v_j(\mathbf{g}) g_i] e^{i\mathbf{g} \cdot \mathbf{r}} d^3\mathbf{g} \tag{18}$$

where  $v_i(\mathbf{g})$  is the  $i$ th component of the displacement. The corresponding elastic stress is given by equation (4). The homogeneous strain in equation (16) and equation (4) is determined by the boundary constraint. If the boundary is constrained so that the system is not allowed to have any homogeneous deformation, the homogeneous strain,  $\bar{\epsilon}_{ij}$ , is equal to zero. In this case, the whole system is stressed. Similarly, if the system is subject to an initial applied strain,  $\epsilon_{ij}^{\text{a}}$ , then the boundary is held fixed,  $\bar{\epsilon}_{ij} = \epsilon_{ij}^{\text{a}}$ . On the other hand, if the system is stress-free, i.e., the system is allowed to deform so that the average stress in the system is zero, the homogeneous strain is obtained by minimizing the total elastic energy with respect to the homogeneous strain. In this work, we consider the simple case that the boundary is constrained so that the homogeneous strain is zero. The cases of constant applied strain and applied stress will be discussed elsewhere.

### 3. DIFFUSION EQUATION IN ELASTICALLY INHOMOGENEOUS SYSTEMS

For a binary substitutional solid solution, the diffusion flux (in unit of atoms per unit area per unit time) is given by

$$J = -N_v M \nabla \mu \tag{19}$$

where  $N_v$  is the number of atoms per unit volume,  $M$  is a mobility given by

$$M = X(1-X)[XM_1 + (1-X)M_2] \tag{20}$$

where  $X$  is the composition of species 2 (mole or atom fraction),  $M_1$  and  $M_2$  are atomic mobilities of species 1 and 2, respectively. They are related to the diffusivity through

$$M_i = \frac{D_i}{k_B T}$$

where  $k_B$  is the Boltzmann constant,  $T$  is the temperature, and  $D_i$  is the diffusion coefficient of species  $i$  in a dilute solution. For simplicity, we assume that the mobilities of the two species are equal, and thus

$$M = \frac{DX(1-X)}{k_B T}.$$

In a compositionally inhomogeneous solid solution with composition-dependent lattice parameter,  $\mu$  is given by

$$\mu(\mathbf{r}) = \frac{\partial f(X)}{\partial X} - \alpha \nabla^2 X + \mu_{\text{el}} \tag{21}$$

where  $f(X)$  is the incoherent free energy density of the solid solution,  $\alpha$  is the gradient energy coefficient [39], and

$$\mu_{\text{el}} = \frac{1}{N_v} \frac{de_{\text{el}}}{dX}$$

is the elastic potential due to the coherency strain, and is given by

$$\begin{aligned}
N_v \mu_{\text{el}} &= -\lambda_{ijkl}^{\circ} (\bar{\epsilon}_{ij} + \delta \epsilon_{ij}(\mathbf{r})) \epsilon_{kl}^{\circ} + \lambda_{ijkl}^{\circ} \epsilon_{ij}^{\circ} \epsilon_{kl}^{\circ} \delta X(\mathbf{r}) + \\
&\quad \frac{1}{2} \lambda'_{ijkl} (\bar{\epsilon}_{ij} + \delta \epsilon_{ij}(\mathbf{r})) (\bar{\epsilon}_{kl} + \delta \epsilon_{kl}(\mathbf{r})) \\
&\quad - 2\lambda'_{ijkl} (\bar{\epsilon}_{ij} + \delta \epsilon_{ij}(\mathbf{r})) \epsilon_{kl}^{\circ} \delta X(\mathbf{r}) + \frac{3}{2} \lambda'_{ijkl} \epsilon_{ij}^{\circ} \epsilon_{kl}^{\circ} (\delta X(\mathbf{r}))^2
\end{aligned} \tag{22}$$

where  $\delta \epsilon_{kl}(\mathbf{r})$  is given by (18).

The time-dependent diffusion equation is then given by

$$\frac{dX(\mathbf{r})}{dt} = \nabla \left[ \frac{DX(1-X)}{k_B T} \right] \nabla \left[ \frac{df(X)}{dX} - \alpha \nabla^2 X + \mu_{\text{el}} \right] \tag{23}$$

Although the above variable-coefficient diffusion equation can be efficiently solved using the semi-implicit Fourier-Spectral method [40], to avoid unnecessary discussions on the numerical method, we make a further simplification by assuming that the factor  $X(1-X)$  is a constant given by  $X_o(1-X_o)$  where  $X_o$  is the overall composition.

Using the dimensionless units,

$$\begin{aligned} t^* &= \frac{DtX_o(1-X_o)}{(\Delta x)^2}, f^* = \frac{f}{k_B T} \\ \mu_{el}^* &= \frac{\mu_{el}}{k_B T} \nabla^* = (\Delta x)^2 \nabla, \\ r^* &= \frac{r}{\Delta x}, \text{ and } \kappa^* = \frac{\kappa}{k_B T (\Delta x)^2} \end{aligned}$$

we have

$$\frac{dX}{dt^*} = (\nabla^*)^2 \left[ \frac{df^*(X)}{dX} - \alpha^* (\nabla^*)^2 X + \mu_{el}^* \right] \quad (24)$$

Taking a Fourier-transform of both sides of equation (24), we have the temporal evolution of the composition wave amplitude,  $X(\mathbf{g})$ ,

$$\begin{aligned} \frac{dX(\mathbf{g}^*)}{dt^*} &= -(g^*)^2 \\ &\left[ \left( \frac{df^*(X)}{dX} \right)_{\mathbf{g}^*} + \alpha^* (g^*)^2 X(\mathbf{g}^*) + \mu_{el}^*(\mathbf{g}^*) \right] \end{aligned} \quad (25)$$

where  $g^*$  is the magnitude of  $\mathbf{g}^*$ ,  $X(\mathbf{g}^*)$  and  $\mu_{el}(\mathbf{g}^*)$  are the Fourier transforms of  $X(\mathbf{r}^*)$  and  $\mu_{el}^*(\mathbf{r}^*)$ , respectively. The above equation is most efficiently solved using a semi-implicit method [40],

$$\begin{aligned} X(\mathbf{g}^*, t^* + \Delta t^*) &= \\ \frac{X(\mathbf{g}^*, t^*) - \Delta t^* (g^*)^2 \left[ \left( \frac{df^*(X)}{dX} \right)_{\mathbf{g}^*} + \mu_{el}^*(\mathbf{g}^*) \right]}{1 + \Delta t^* \alpha^* (g^*)^4} \end{aligned} \quad (26)$$

where  $\Delta t^*$  is the time step for integration. Algorithms with higher order in  $t$  are also available [40].

## 4. DISCUSSION

### 4.1. Convergence of the proposed method

In principle, the convergence and accuracy of the proposed perturbation method for a given order of approximation can be tested against analytical solutions which are available for certain special precipitate shapes [2]. However, the analytical solutions are available only for systems with a sharp-interface description whereas the interfaces in our numerical calculation are diffuse. Therefore, to examine the

accuracy, we compare the results from the proposed method with those obtained from an independent calculation using a conjugate gradient method (CGM) with the same diffuse-interface description [37]. In CGM, the elastic equation is numerically solved until the results converge.

For discussion, we consider a model binary alloy with its chemical thermodynamics described by the following local incoherent free energy density,

$$f^*(X) = -(X-0.5)^2 + 2.5(X-0.5)^4 \quad (27)$$

where  $X$  is composition. The equilibrium compositions determined from equation (27) are 0.053 and 0.947, respectively. We introduce a circular precipitate with composition 0.947 and a radius of  $R = 10$  in a square domain of matrix ( $256 \times 256$ ) with composition 0.053. Periodic boundary conditions are applied along both Cartesian axes. The initially sharp composition profile describing the precipitate is allowed to relax for a certain number of time steps by solving the Cahn-Hilliard diffusion equation with a gradient energy coefficient, 1.5, but without including the stress effect. The resulting two-dimensional diffuse compositional profile is then used to calculate the stress distributions using the proposed perturbation method with different orders of approximation and the CGM [37]. For comparing the results, the number of time steps to relax the profile is not particularly important since we use the same profile for the two independent calculations. Both calculations employed the spectral method for the spatial discretization of the elasticity equation. The composition expansion coefficient,  $\epsilon_o$  is chosen to be 0.05. The elastic constants used are  $C_{11}^o = 300$ ,  $C_{12}^o = 100$ ,  $C_{44}^o = 100$ , and  $C'_{11} = 150$ ,  $C'_{12} = 50$ ,  $C'_{44} = 50$  for a hard precipitate and  $C'_{11} = -150$ ,  $C'_{12} = -50$ ,  $C'_{44} = -50$  for a soft precipitate, all in units of  $N/k_B T$ . This set of elastic constants produce more than 50% difference in the elastic constants between the precipitate and matrix, which is artificially large compared to the typical elastic inhomogeneity in most of the practical two-phase alloys.

Examples of equilibrium stress distributions,  $\sigma_{xx}$  and  $\sigma_{yy}$ , as a function of position along a line cut through the center of the precipitate in the  $x$  direction are shown in Fig. 1 for a hard precipitate, and Fig. 2 for a soft precipitate. The shear component,  $\sigma_{xy}$ , is zero along that line, so it is not shown. In both Figs 1 and 2, the squares and circles represent the results from the proposed perturbation method and the crosses and pluses represent those from the CGM. It can be seen that for both hard and soft precipitates, the results from two calculations agree very well for both stress components. Both calculations converge to essentially the same results although the two calculations were performed using two entirely independent computer codes. It is shown that although the stresses in the matrix are similar for both the hard

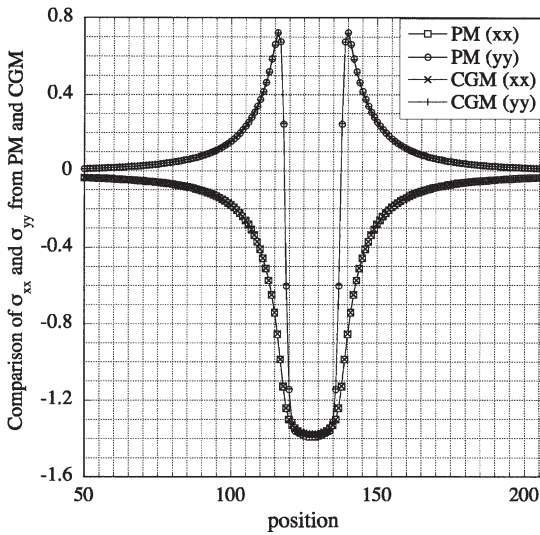


Fig. 1. Stress distributions along the  $x$ -direction across the center of a hard precipitate. The open squares and circles represent the  $xx$  and  $yy$  components obtained from the proposed perturbation method (PM). The crosses and pluses represent the corresponding results from a conjugate gradient method (CGM).

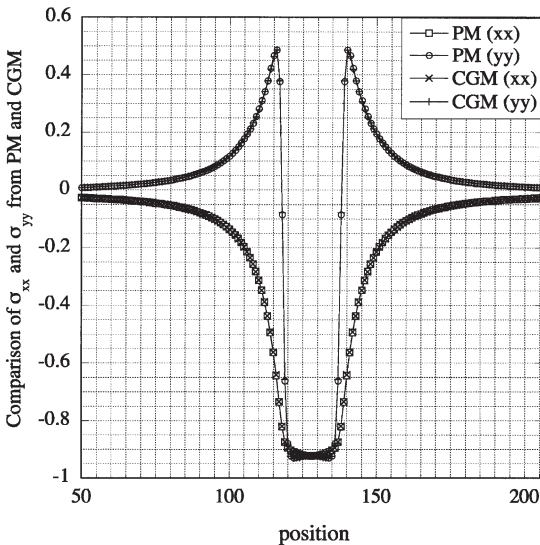


Fig. 2. Stress distributions along the  $x$ -direction across the center of a soft precipitate. The open squares and circles represent the  $xx$  and  $yy$  components obtained from the proposed perturbation method (PM). The crosses and pluses represent the corresponding results from a conjugate gradient method (CGM).

and soft precipitates, the absolute magnitude within the hard precipitate is significantly higher than that within the soft precipitate. It is easily understandable since we used exactly the same two-dimensional compositional profile for the hard and soft precipitates and the larger elastic constants for the hard precipitates would produce larger stresses. To examine the convergence of the elastic solution as a function of iteration number, or the order of approximation, the

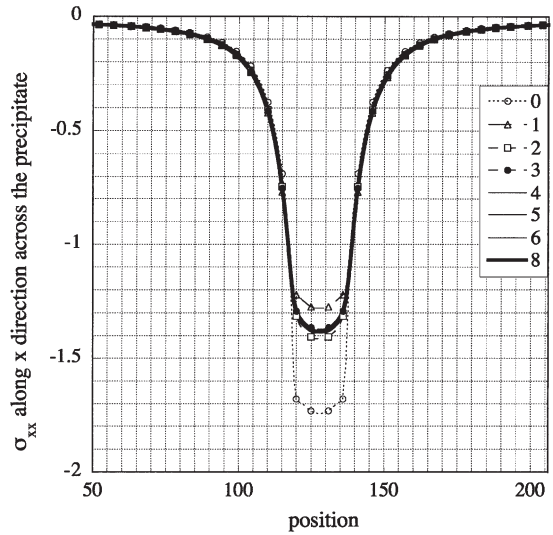


Fig. 3. The  $xx$  component of the elastic stress along the  $x$ -direction across the center of the hard precipitate as a function of iteration numbers (or the order of approximations) from the perturbation iterative method.

stress components,  $\sigma_{xx}$  and  $\sigma_{yy}$ , as a function of position for a given composition profile are plotted for different iteration numbers in Figs 3–6 for both hard and soft precipitates. We used the same materials parameters as in Figs 1 and 2. In calculating the stress distributions, the elastic displacements and thus the elastic strains were obtained using various orders of approximations, with the stress calculated using equation (4). For example, in the legends for the figures, the number “0” represents the case that the elastic solution,  $\epsilon_{ij}(\mathbf{r})$ , was obtained using the zeroth-order approximation (11), but the elastic constants used in

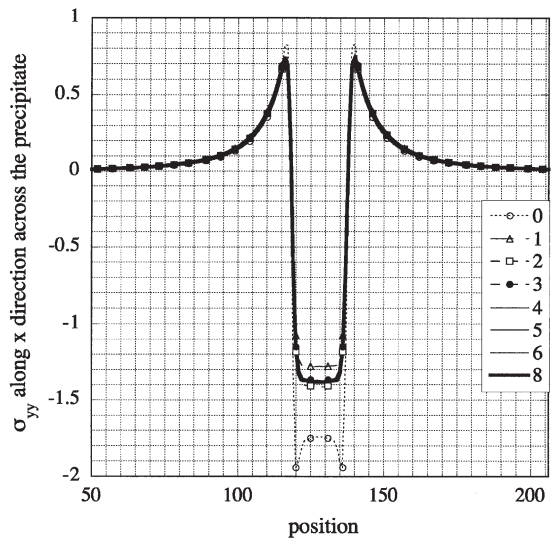


Fig. 4. The  $yy$  component of the stress along the  $x$ -direction across the center of the hard precipitate as a function of iteration numbers (or the order of approximations) from the iterative method.

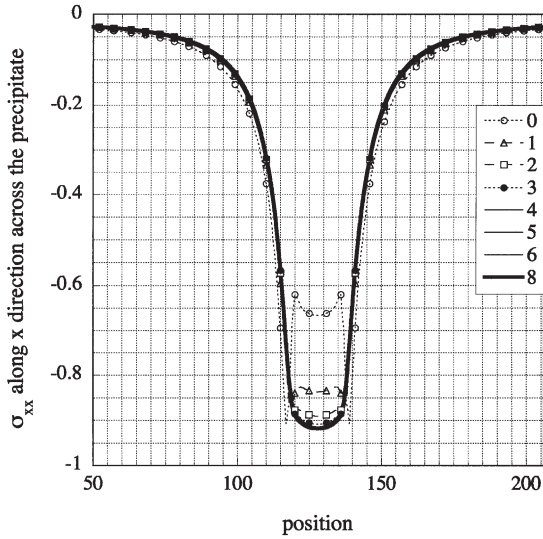


Fig. 5. The  $xx$  component of the stress along the  $x$ -direction across the center of the soft precipitate as a function of iteration numbers (or the order of approximations) from the iterative method.

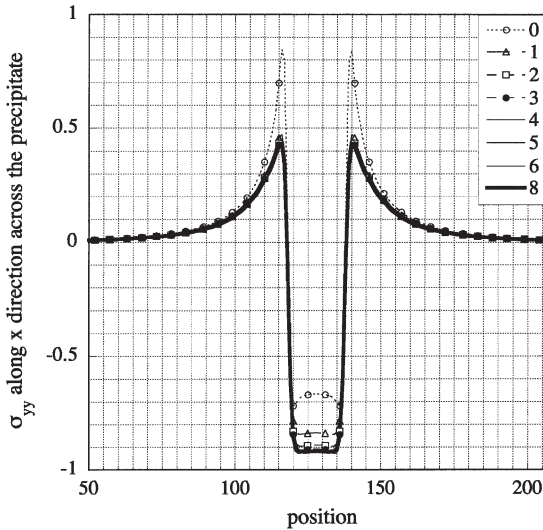


Fig. 6. The  $yy$  component of the stress along the  $x$ -direction across the center of the soft precipitate as a function of iteration numbers (or the order of approximations) from the iterative method.

calculating the stress distributions in equation (4) are not homogeneous. Therefore, even with the zeroth order of approximation, some degree of elastic inhomogeneity has been taken into account in the elastic energy calculation. As a matter of fact, the level of approximation used in Koyama’s simulation for elastically inhomogeneous systems [27] corresponds to our zeroth order approximation. As one can see from Figs 3–6, even with such a large elastic inhomogeneity,  $\approx 50\%$ , considered in the calculations, the elastic stress essentially converges after three to four iterations, indicating a third or fourth

order approximation will be sufficient for the elastic energy calculations with a similar degree of elastic inhomogeneity assumed in this calculation. The zeroth order approximation overestimates the stress within the hard precipitate and underestimates the stress within the soft precipitate by about 25–30%. The error is reduced to 10% with a first order approximation. Table 1 shows the required iteration numbers or order of approximation to get converged elastic solution for a given ratio of elastic constants between precipitate and matrix. As expected, the number of iterations increases with the degree of elastic inhomogeneity. For a 10% elastic inhomogeneity, it is sufficient to use the first order approximation. Even with inhomogeneities as large as 100%, it requires only about five iterations.

#### 4.2. Efficiency of the proposed method

Since each order of the approximation for the elastic solution is obtained analytically (see equations (11) and (14)), the proposed algorithm is extremely efficient. Table 2 lists the relative computation time required for each order of approximation as compared to the zeroth order approximation. As one can see, a first-order approximation requires about only 50% more time than the homogeneous approximation. Even for the extremely large inhomogeneity case, the computation time required is about 4 times that for the zeroth-order or homogeneous approximation. A CGM for the same problem will typically take 5–6 times longer than the proposed perturbation method [37]. Furthermore, since we solve both the elastic equation and the Cahn–Hilliard diffusion equation in Fourier space, it is straightforward to implement a semi-implicit algorithm for numerical integration with respect to time. We found that with the semi-implicit algorithm, time steps as much as 500 times larger can be used as compared to the explicit Euler method [40]. Therefore, our proposed combination of iterative perturbation method for the elastic equation and the semi-implicit spectral algorithm for the diffusion equation is very efficient for modeling microstructure evolution in elastically inhomogeneous systems.

#### 4.3. Morphological dependence on elastic inhomogeneity

##### 4.3.1. Shapes of isolated precipitates.

The shapes of a single coherent precipitate in elastically inhomogeneous systems have been studied previously [32, 34, 35]. As an example of applying the proposed iterative perturbation algorithm, we study the shape evolution of a single precipitate and examine the shape dependence of a precipitate on elastic inhomogeneity. The shape evolution of an isolated particle towards equilibrium is obtained by solving the Cahn–Hilliard diffusion equation with elastic stress. We used a  $256 \times 256$  grid. The initial composition within the precipitate is assigned the equilibrium value determined from the local incoherent free energy den-

Table 1. Convergence of the iterative method

$\frac{C_{ij}^P}{C_{ij}^M}$	0.19	0.37	0.55	0.73	0.91	1.0	1.09	1.27	1.45	1.63	1.99
Iterations	5	4	3	2	1	0	1	2	3	4	5

Table 2. Computational time required for a given number of iterations normalized by the time required for the zeroth order approximation

Iterations	0	1	2	3	4	5	6
Time	1.0	1.5	2.1	2.6	3.1	3.7	4.3

sity function,  $X = 0.947$ , whereas  $X = 0.06$  in the matrix which is higher than the incoherent equilibrium composition, 0.053. The coherent equilibrium compositions are not known in advance and will be automatically achieved during the temporal evolution towards equilibrium. The time step for integrating the Cahn–Hilliard equation is 0.5 and the gradient energy coefficient is 1.5. The composition expansion coefficient is 0.05. We consider a cubically anisotropic system. We choose a set of elastic constants which provide an elastic anisotropy typical of those Ni-based superalloys. In particular, we use the following values for the elastic constants in reduced units:  $C_{11} = 232$ ,  $C_{12} = 153$  and  $C_{44} = 117$  [41]. To examine the effect of elastic inhomogeneity, we artificially keep the bulk modulus ( $B = C_{11} + C_{12}$  for the plane problem) and the ratio of anisotropy ( $\delta = 2C_{44}/(C_{11} - C_{12})$ ) the same in the matrix and precipitate, while changing the ratio of shear modulus  $\kappa = C_{44}^P/C_{44}^M$  in which P and M denote the precipitate and matrix, respectively. As an example, the temporal evolution of a soft precipitate with  $\kappa = 0.3$  from the initially circular precipitate ( $R = 40$ ) is shown in Fig. 7. The composition distributions along the  $x$ -direction and the diagonal direction passing through the center of the precipitate are plotted as a function of time in Fig.

8. It is well known that the shape of the particle is controlled by the total of interfacial energy and elastic strain energy. In this particular example, the interfacial energy is assumed to be isotropic, so the development of anisotropic particle shape is entirely due to the anisotropic elastic interactions caused by the lattice mismatch and elastic inhomogeneity. The softness of the precipitate and the cubic anisotropy result in the elongation of the particle along the  $[11]$  and  $[\bar{1}\bar{1}]$  directions. A very similar shape change was observed by Lee using the discrete atom method [31,

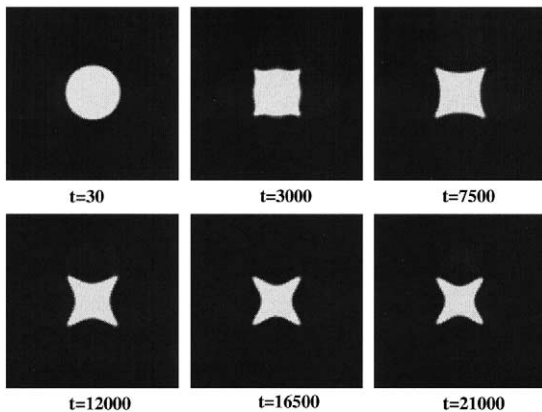


Fig. 7. The particle shape as a function of time for a soft precipitate ( $\kappa = 0.3$ ,  $R = 40$ ).

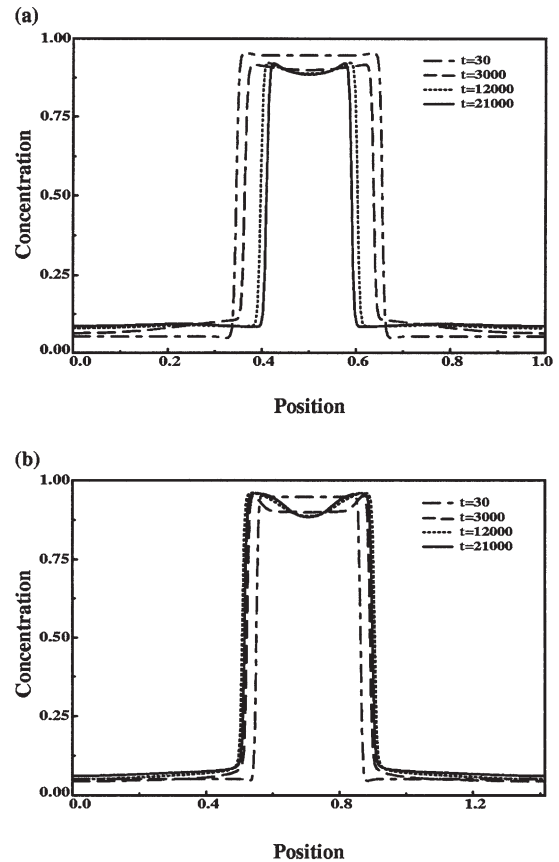


Fig. 8. Evolution of compositional profiles as a function of time for a soft precipitate ( $\kappa = 0.3$ ,  $R = 40$ ), (a) along the  $x$ -direction, (b) along the diagonal direction.

32]. The coherent composition within the precipitate is lower than the initially assigned value (the incoherent equilibrium composition of the precipitate) whereas in the matrix the composition is higher than the initial incoherent equilibrium composition. The composition distribution inside the precipitate is highly inhomogeneous due to the presence of coherent stress. There is no significant change in the shape of the precipitate and the composition distribution inside the precipitate after about  $t = 16,500$ . However, due to the application of the periodic boundary conditions and the slow solute redistribution towards equilibrium, the last morphology shown in Fig. 7 is close to, but not exactly the equilibrium shape of an isolated precipitate. Precipitate shape as a function of elastic inhomogeneity ( $\kappa = 1.70, 1.35, 1.00, 0.60, 0.45$  and  $0.30$ ) is shown in Fig. 9. They all started with an initially circular precipitate with radius 40. For an elastically homogeneous precipitate, the equilibrium shape is cubic with rounded corners. With the decrease in  $\kappa$ , i.e., when the precipitate becomes softer than the matrix, the boundaries of the cuboid along the  $[100]/[010]$  directions become concave, whose curvature strongly depends on the ratio of shear modulus  $\kappa$ . The hard precipitate has convex boundaries, but the dependence of equilibrium shape on  $\kappa$  is rather weak compared to the elastically soft precipitate. Existing studies using other computational approaches predicted similar results [31, 32, 34].

**4.3.2. Dependence of a two-phase morphology on elastic inhomogeneity.** In order to characterize the elastic inhomogeneity of a two-phase cubic system, we use three quantities, the bulk modulus ( $B = C_{11} + C_{22}$ ), the shear modulus ( $G = 2C_{44}$ ), and the anisotropy ( $\delta = 2C_{44}/(C_{11} - C_{12})$ ). We examined the inhomogeneity effect of each of these three quantities by holding the other two constant. In the first case, the bulk and shear moduli are homogeneous while the bulk modulus is a function of composition. As an example, the moduli are set to be  $C_{11} = 300$ ,

$C_{12} = 160$  and  $C_{44} = 70$ . We use the same bulk modulus ( $B = 460$ ) and the shear modulus ( $G = 140$ ) for the two phases, and change their anisotropy ratio ( $\delta^P = 1.00, 1.14, 1.34, 1.63, 2.05, 2.80$ ,  $\delta^M = 1.00, 0.89, 0.79, 0.72, 0.66, 0.61$ ). The angular-dependent Young's moduli as a function of direction for the precipitate, the matrix and a uniform solid solution are plotted in Fig. 10(a) for the case of  $\delta^P = 2.80$  and  $\delta^M = 0.61$ . For cubic systems, Young's modulus  $E(\theta)$  is given by

$$E(\theta) = \frac{1}{4}(3C_{11} + C_{12} + 2C_{44}) + (C_{11} - C_{12} - 2C_{44} \cos(4\theta)) \quad (28)$$

where  $\theta$  is the angle with respect to the elastic main axis. It is easy to see from Fig. 10(a) that the Young's moduli along  $[11]$  and  $[1\bar{1}]$  directions are the same for both phases while the precipitate has larger modulus than the matrix along the  $[01]$  and  $[10]$  directions.

The morphological dependence of a phase-separated two-phase system on the anisotropy ratio is shown in Fig. 11. In the simulations, the gradient energy coefficient, composition expansion coefficient, and the time increment for integration are the same as in the last example for a single precipitate evolution. The simulations were started with an average concentration of 0.5 with a small random concentration fluctuation. The white regions in Fig. 11 stand for the phase with larger Young's moduli along the  $[10]$  and  $[01]$  directions than the black regions. It is shown that with an increase in difference in the moduli between the two phases, the phase with larger moduli becomes disconnected and forms isolated cuboidal composition domains. It is worth pointing out that although the elastically soft direction for the precipitate phase in Fig. 11(f) is along  $[11]$  and  $[1\bar{1}]$  directions, the overall spatial distribution of the isolated domains displays alignment along the  $[10]$  and  $[01]$  directions. As expected, when the anisotropy for both the precipitate and matrix is rotated by  $45^\circ$ , the hard phase still appears as isolated precipitates but the alignment is now along the  $[11]$  and  $[1\bar{1}]$  directions.

In the second case, the bulk modulus and the anisotropy are the same for the precipitate and matrix phases while the shear modulus is a function of composition. In the numerical example, we use  $C_{11} = 300$ ,  $C_{12} = 200$  and  $C_{44} = 100$ ,  $B = 500$  and  $\delta = 2$ . The ratios of shear modulus between the two phases are  $\kappa = 1.0, 1.2, 1.5, 1.9, 2.6, 3.6$ . The Young's moduli as a function of direction for the precipitate, the matrix and a uniform solid solution are plotted in Fig. 10(b) for the case of  $\kappa = 3.6$ . In this case, one phase is harder than the other in all directions. Figure 12 presents the morphological dependence on elastic inhomogeneity for this case. The result is quite similar to the first case. At large inhomogeneity, the harder phase consists of isolated par-

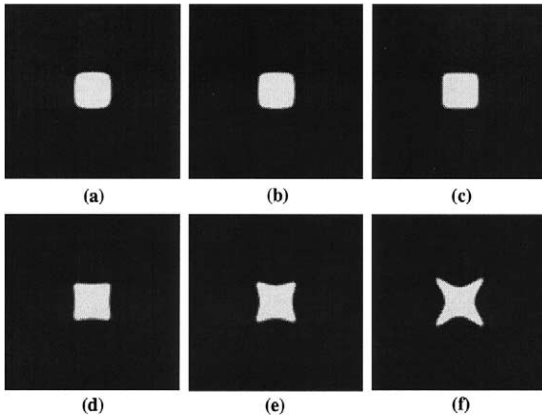


Fig. 9. The shape of an isolated precipitate as a function of elastic inhomogeneity ((a)  $\kappa = 1.70$ , (b)  $\kappa = 1.35$ , (c)  $\kappa = 1.00$ , (d)  $\kappa = 0.60$ , (e)  $\kappa = 0.45$ , (f)  $\kappa = 0.3$ ).

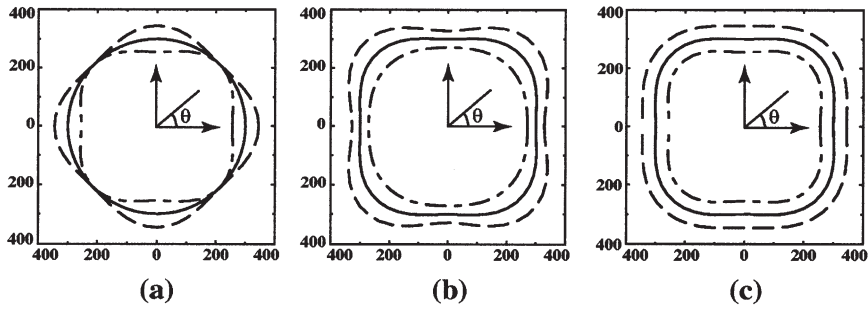


Fig. 10. Young's modulus as a function of direction: dot-dashed line—matrix; dashed line—precipitate; and solid line—a homogeneous solution. (a) Homogeneous bulk and shear moduli but inhomogeneous anisotropy; (b) homogeneous bulk modulus and anisotropy but inhomogeneous shear modulus; (c) homogeneous shear modulus and anisotropy but inhomogeneous bulk modulus.

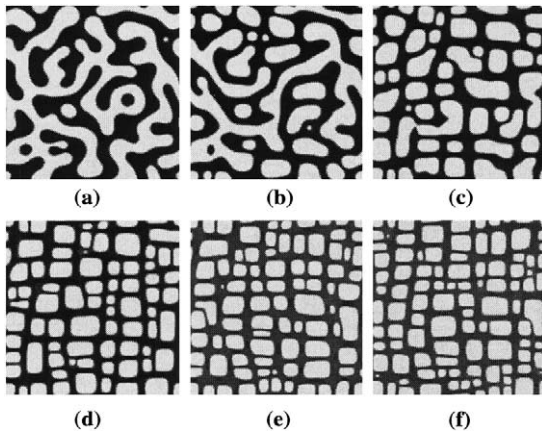


Fig. 11. Two-phase morphology as a function of elastic inhomogeneity caused by different degrees of elastic anisotropy in the matrix and precipitate ( $\delta^P$ ,  $\delta^M$ ): (a) (1.00, 1.00), (b) (1.14, 0.89), (c) (1.34, 0.79), (d) (1.63, 0.72), (e) (2.05, 0.66), (f) (2.80, 0.61). Both the bulk and shear moduli are homogeneous.

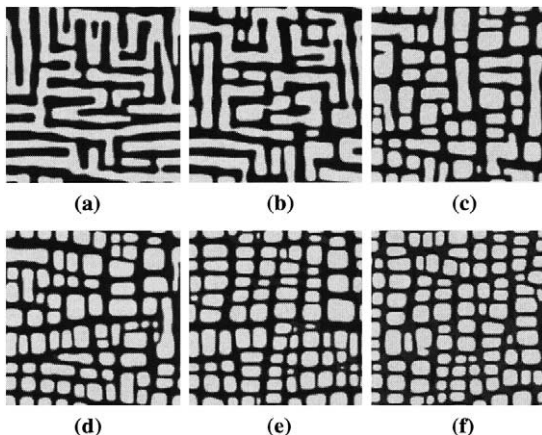


Fig. 12. Two-phase morphology as a function of elastic inhomogeneity caused by different shear moduli in the two phases ((a)  $\kappa = 1.0$ , (b)  $\kappa = 1.2$ , (c)  $\kappa = 1.5$ , (d)  $\kappa = 1.9$ , (e)  $\kappa = 2.6$ , (f)  $\kappa = 3.6$ ). The precipitate and matrix have the same bulk moduli and the same degree of elastic anisotropy.

ticles and the softer phase is a connected matrix wrapping the hard phase. The particles are aligned along the elastically soft directions, [10] and [01]. The temporal morphological evolution during phase separation of a homogeneous solid solution to a two-phase mixture is shown in Fig. 13. The morphology [Fig. 13(a)] during the initial stage of phase separation is very similar to spinodal phase separation without elastic interactions. As the phase separation process progresses, morphological alignment along the elastically soft directions developed. With further coarsening, the initially interconnected hard phase breaks into isolated particles.

In the third case, the shear modulus and anisotropy are independent of composition while the bulk modulus varies with composition. Figure 10(c) shows the Young's moduli as a function of direction for the hard and soft phases. In this case, the degree of elastic inhomogeneity has essentially no effect on the morphology. Figure 14 shows morphologies with two different ratios of bulk moduli between the two phases.

It should be emphasized that although previous computer simulations [25, 26, 27, 30] using first-order approximations predicted similar morphological dependence on elastic inhomogeneity as shown above, there are a number of differences between prior first-order simulations and the present work using high-order approximations. First, in prior simulation using first-order approximations, the degree of elastic inhomogeneity is not clear whereas in the present work it is shown that it requires more than about 50% difference in modulus in the two phases (see Fig. 12) to yield a two-phase morphology which is significantly different from the homogeneous case. Secondly, although the first-order approximations predict the qualitatively correct two-phase morphology, the local stress distributions described by a first-order approximation for a system with large elastic inhomogeneity can be in serious error. As a result, the elastic energy contribution to the driving force for microstructure evolution such as coarsening for two-phase systems is not accurately determined in a first-order approximation. Furthermore, if one is interested

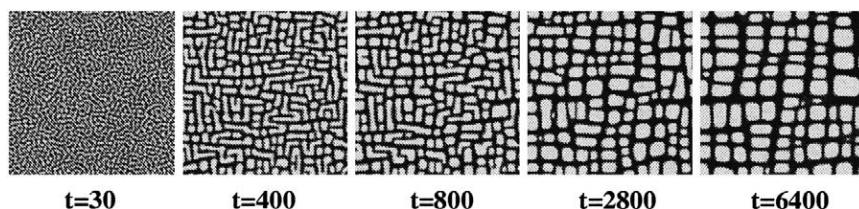


Fig. 13. Temporal evolution during phase separation of a homogeneous solid solution into a two phase mixture for the case of elastic inhomogeneity caused by different shear moduli in the two phases,  $\kappa = 2.6$ . The precipitate and matrix have the same bulk moduli and the same degree of elastic anisotropy.

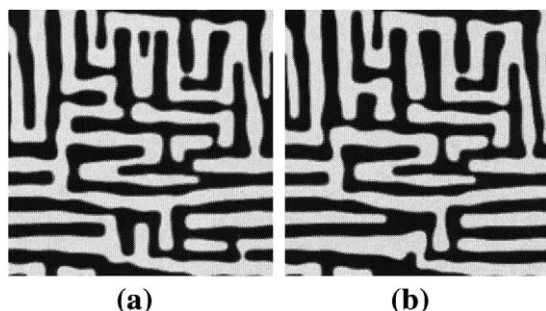


Fig. 14. Two-phase morphology as a function of elastic inhomogeneity caused by different bulk moduli in the two phases ((a)  $B^p/B^M = 1.0$ , (b)  $B^p/B^M = 1.5$ ). The precipitate and matrix have the same shear moduli and the same degree of elastic anisotropy.

in calculating the effective modulus of a two-phase mixture, a first-order approximation will result in inaccurate results except for systems with small elastic inhomogeneity ( $< \sim 10\%$ ).

## 5. SUMMARY

A diffuse-interface field model is proposed for predicting the morphological and microstructural evolution in elastically anisotropic systems with strong elastic inhomogeneities. Within this model, the elastic solutions are obtained using an iterative method with each iteration corresponding to a given order of approximation in Khachaturyan's perturbation method. Highly accurate results can be obtained using various orders of approximations for different degrees of elastic inhomogeneity. We compared the results with various orders of approximation with those obtained from a conjugate gradient method. It is shown that first-order approximation is reasonable if the elastic inhomogeneity is less than about 10%. Even for systems with extremely large elastic inhomogeneities (100%), the proposed method requires less than five iterations. A combination of the iterative perturbation method for the mechanical equilibrium equation and a semi-implicit spectral method for the Cahn-Hilliard equation results in an extremely efficient model for studying morphological evolution in coherent systems with large elastic inhomogeneities. We conclude that for strong elastic inhomogeneity ( $> \sim 20\%$ ), first-order approximations predicted

qualitatively correct two-phase morphologies whereas the local stress distributions and thus the driving force for coarsening of such a two-phase system can be in serious error. We also showed that it requires a rather strong elastic inhomogeneity ( $> \sim 50\%$ ) to produce precipitate morphologies that are dramatically different from elastically homogeneous systems.

*Acknowledgements*—The authors are grateful for the financial support from the NSF under grant No. DMR-96-33719. The simulations were performed at the San Diego Supercomputer Center and the Pittsburgh Supercomputing Center.

## REFERENCES

1. Khachaturyan, A. G., *Theory of Structural Transformations in Solids*. Wiley, New York, 1983.
2. Mura, T., *Micromechanics in Solids*. Kluwer Academic, Dordrecht, 1982.
3. Doi, M., *Prog. Mater. Sci.*, 1996, **40**, 79.
4. Fratzl, P., Penrose, O. and Lebowitz, J. L., *J. Stat. Phys.*, 1999, **95**, 1429.
5. Chen, L. Q., Wang, Y. Z. and Khachaturyan, A. G., *Phil. Mag. Lett.*, 1991, **64**, 241.
6. McCormack, M., Khachaturyan, A. G. and Morris, J. W. Jr., *Acta metall. mater.*, 1992, **40**, 325.
7. Chen, L. Q., Wang, Y. Z. and Khachaturyan, A. G., *Phil. Mag. Lett.*, 1992, **65**, 15.
8. Wang, Y., Chen, L. Q. and Khachaturyan, A. G., *Acta metall. mater.*, 1995, **41**, 279.
9. Abinandanan, T. A. and Johnson, W. C., *Acta metall. mater.*, 1993, **41**, 17.
10. Abinandanan, T. A. and Johnson, W. C., *Acta metall. mater.*, 1993, **41**, 27.
11. Thompson, M. E., Su, C. S. and Voorhees, P. W., *Acta metall. mater.*, 1994, **42**, 2107.
12. Nambu, S. and Sagala, D. A., *Phys. Rev. B*, 1994, **50**, 5838.
13. Wang, Y. Z., Wang, H. Y., Chen, L. Q. and Khachaturyan, A. G., *J. Am. Ceram. Soc.*, 1992, **78**, 657.
14. Fan, D. N. and Chen, L. Q., *J. Am. Ceram. Soc.*, 1995, **78**, 1680.
15. Su, C. H. and Voorhees, P. W., *Acta mater.*, 1996, **44**, 1987.
16. Su, C. H. and Voorhees, P. W., *Acta mater.*, 1996, **44**, 2001.
17. Wang, Y. and Khachaturyan, A. G., *Acta mater.*, 1997, **45**, 759.
18. Hu, H. L. and Chen, L. Q., *J. Am. Ceram. Soc.*, 1998, **81**, 492.
19. Semenovskaya, S. and Khachaturyan, A. G., *J. Appl. Phys.*, 1998, **83**, 5125.
20. Li, D. Y. and Chen, L. Q., *Acta metall. mater.*, 1998, **46**, 639.
21. Le Bouar, Y., Loiseau, A. and Khachaturyan, A. G., *Acta mater.*, 1998, **46**, 2777.

22. Wen, Y. H., Wang, Y. and Chen, L. Q., *Acta mater.*, 2000, **47**, 4375.
23. Johnson, W. C. and Voorhees, P. W., *J. Appl. Phys.*, 1986, **61**, 1610.
24. Onuki, A., *J. Phys. Soc. Jpn*, 1989, **58**, 3065.
25. Nishimori, H. and Onuki, A., *Phys. Rev. B*, 1990, **42**, 980.
26. Sagui, C., Somoza, A. M. and Desai, R., *Phys. Rev. E*, 1994, **50**, 4865.
27. Koyama, T., Miyazaki, T. and Mebed, A. E., *Metal. Mater. Trans. A*, 1995, **26**, 2617.
28. Li, D. Y. and Chen, L. Q., *Scripta mater.*, 1997, **37**, 1271.
29. Laberge, C. A., Fratzl, P. and Lebowitz, J. L., *Acta mater.*, 1997, **45**, 3949.
30. Sagui, C., Orlikowski, D., Somoza, A. and Roland, C., *Phys. Rev. E*, 1998, **58**, 569.
31. Lee, J. K., *Metal. Mater. Trans. A*, 1995, **27**, 1449.
32. Lee, J. K., *Mater. Trans. JIM*, 1998, **39**, 114.
33. Schmidt, I. and Gross, D., *J. Mech. Phys. Solids*, 1997, **45**, 1521.
34. Schmidt, I., Muellerand, R. and Gross, D., *Mech. Mater.*, 1998, **30**, 181.
35. Jou, H. J., Leo, P. H. and Lowengrub, J. S., *J. Comput. Phys.*, 1997, **131**, 109.
36. Leo, P. H., Lowengrub, J. S. and Hou, H. J., *Acta mater.*, 1998, **61**, 2113.
37. Zhu, J. Z., Shen, J., Tikare, V. and Chen, L. Q., *Model. Sim. Mat. Sci. Eng.*, 2001, submitted for publication.
38. Khachatryan, A. G., Semenovskaya, S. and Tsakalakos, T., *Phys. Rev. B*, 1996, **52**, 15909.
39. Cahn, J. W. and Hilliard, J. E., *J. Chem. Phys.*, 1958, **28**, 258.
40. Chen, L. Q. and Shen, J., *Comput. Phys. Commun.*, 1998, **108**, 147.
41. Paris, O., Langmanyr, F., Vogl, G. and Fratzl, P., *Z. Metallkd.*, 1995, **86**, 860.